

A novel approach for enhancing thermal performance of Battery Modules based on Finite Element Modelling and Predictive modelling mechanism

¹Akhil Garg, ^{1,2}C. Ruhatiya, ³Xujian Cui, Xiongbin Peng³, Yogesh Bhalerao^{4,5}, *¹Liang Gao

¹State Key Lab of Digital Manufacturing Equipment & Technology, School of Mechanical Science and Engineering, Huazhong University of Science and Technology, Wuhan, China

²School of Engineering Sciences, Mahindra École Centrale, Hyderabad, Telangana 500043, India

³Intelligent Manufacturing Key Laboratory of Ministry of Education, Shantou University, Shantou, China

⁴Department of Mechanical Engineering, MIT Academy of Engineering (MAE), Pune MH 412105, India

⁵Engineering Faculty of Science, University of East Anglia, Norwich Reserch Park, Norwich NR47TJ

Abstract

Electric Vehicles (EVs) are estimated as the most sustainable solutions for future transportation requirements. However, there are various problems related to the battery pack module and one of such problem is invariable high-temperature differences across the battery pack module due to the discharging and charging of batteries under operating conditions of EVs. High-temperature differences across the battery module contribute to degradation of maximum charge storage and capacity of Li-ion batteries which ultimately affects the performance of EVs. To address this problem, a Finite Element Modelling (FEM) based Automated Neural Network Search (ANS) approach is proposed. The research methodology constitutes of the four stages: Design of air-cooled battery pack module, setup of the FEM constraints and thermal equations, formulating the predictive model on generated data using ANS and lastly performing multi-objective response optimization of the best fit predictive model to formulate optimum design constraints for the air-cooled battery module. For efficient thermal management of the battery module, an empirical model is formulated using the mentioned methodology for minimizing the maximum temperature differences, standard deviation of temperature across the battery pack module and battery pack volume. The results obtained are as follows: (1) The battery pack module volume is reduced from 0.003279m^3 to 0.002321m^3 by 29.21%, (2) The maximum temperature differences across the eight cells of battery pack module declines from 6.81K to 4.38K by 35.66%, and (3) The standard deviation of temperature across battery pack decreases from 4.38K to 0.93K by 78.69%. Thus, the predictive empirical model enhances the thermal management and safety factor of battery module.

Keywords: Battery thermal management system; Heat conduction; air cooling; thermal efficiency; Energy storage;

*corresponding author email: gaoliang@mail.hust.edu.cn

43 **1 Introduction**

44 The EVs operated on battery packs has become popular due to there less carbon footprints
45 compared to conventional vehicles and is being highly incentivized by major consumer
46 countries around the world [1-2]. The threat of climate change and increasing dependency on
47 fossil fuels in a long term scenario have started a movement in automotive industry to develop
48 sustainable technologies [3]. EVs are also been seen as a new power sources for electric utilities
49 [4-5]. It cannot be said that EVs are 100% environment friendly, because the electricity needed
50 for charging is still majorly produced from fossil fuels which has large carbon footprints also
51 the metals used in batteries are harmful and rare [6]. However if Well to Wheel (WTW)
52 analysis of EVs and conventional vehicles are compared it can be said that EVs are less
53 polluting if electricity required for charging is generated from renewable energy sources[7].
54 The lithium-ion batteries (LIBs) are preferred as power source of EVs over other types of
55 batteries, because of power requirements of EVs which can be satisfied by LIBs [8-11]. High
56 energy density and long cycling life make LIBs the preferred option for use in EVs [12-13].
57 Set of hundreds of Lithium-ion cells are connected in certain pattern to form a battery pack
58 module such that it provides enough power to maintain driving conditions of EVs [13]. These
59 lithium-ion cells of EVs work at a higher value of discharge rate of current producing enormous
60 heat, which gets confined in battery pack module leading to thermal runaway of Energy Storage
61 System(ESS). This results in temperature rise in the battery pack module and accelerated aging
62 of lithium-ion cells in the pack. Due to these reasons, charge acceptance, energy capability,
63 power capability and reliability of batteries are reduced[14]. However, LIBs have high
64 performance at an upper bound temperature of 45°C and it is observed battery performance
65 increases as the temperature is increased from room temperature to considerably high
66 temperatures(around 45°C)[15]. Also, very low temperature are found to affect the
67 performance of LIBs, at sub-zero temperature LIBs discharge capacity is reduced due to the

68 impedance effect [16] and when charging at high rate while temperature is low, the
69 phenomenon of lithium plating occurs leading to reduced battery life [17]. Its been observed
70 battery pack should have a maximum temperature below 45°C and difference in temperatures
71 between cells in battery pack should be below 5°C to avoid thermal imbalance for a long
72 working life of a battery[15, 18, 19]. Therefore, a thermal management system is required for
73 battery packs to reduce the heat and maintain an optimum favourable temperature inside a
74 battery pack for better performance of LIBs[19-20].

75 Battery pack thermal management is mainly classified into three categories. First, is a natural
76 cooling system where the air is the fluid, heat generated by LIBs is exchanged by natural
77 convection process inside the case[21]. Second, is forced cooling system where fluid can be
78 liquid or air, here forced convection occurs inside battery pack when coolant(liquid or air) is
79 introduced in gaps of cells by an external force, such as fan or blower[21-22]. The forced
80 cooling system has better performance than natural cooling system but natural cooling is more
81 economical than forced cooling, there is a trade-off between factors such as weight, power
82 consumption and economical factor[21]. **Third is the Phase Change Material (PCM) cooling**
83 **system, the PCM system can be a good choice because the latent heat related with melting and**
84 **freezing are capable of storing more heat than sensible thermal storage[23-24].** When Li-ion
85 cells are under working conditions, the PCM will maintain the Li-ion cells at a certain
86 temperature while passively storing the heat. Once the heat generating components (Li-ion
87 cells) are shut-off the PCM will begin to solidify. The PCM based cooling system is efficient
88 in decreasing temperature but there are also challenges for PCMs poor thermal conductivity
89 which decides the thermal transport efficiency, which limits PCMs application where instant
90 response is required to thermal surge [25].

91 Major studies have been carried out using multi-dimensional numerical analysis and thermal
92 resistance models. Certain design configurations of air-cooled battery pack system are

93 numerically modeled and theoretically investigated by Park et al.[26] to get the required
94 thermal specifications. The investigation was conducted on the cooling effect of five different
95 air-flow configuration of a battery system with 36 cells battery pack. It was concluded that the
96 desired cooling performance is attained by using the pressure relief ventilation and tampered
97 manifold without disturbing the design of the existing battery system. Using numerical and
98 analytical modelling the flat-plate battery stacks and cylindrical battery stacks were compared
99 by Xun et al.[27] for getting required air cooling conditions. Two dimensionless parameters,
100 cooling energy efficiency and compactness of battery stacks were varied and, it was concluded
101 that the cylindrical battery stacks were less compact and more efficient under air cooling
102 conditions. Yang et al.[28] concluded that considering design requirement and air cooling
103 conditions, a battery pack in aligned arrangement generates lower temperature compared to a
104 staggered arrangement, but the only drawback is it requires more space comparatively. It is
105 concluded by Wang et al.[29] that when the fan is located on top of the battery pack module,
106 best cooling performance is obtained. Also 5×5 cubic arrangement is proposed for a battery
107 pack with 24/25 arrangement for Li-ion 18650 cells. This occupies lesser space and better
108 cooling is obtained compared to 1×24 and 3×8 arrangements of cells in a battery pack.

109 Previous work of authors has utilized genetic algorithms, support vector machine, response
110 surface method, and surrogate modeling combined with Computational Fluid Dynamics (CFD)
111 tools to address the issue of temperature optimization of battery packs. Li et al.[30] reported
112 simultaneous system volume and cooling performance optimization using CFD based surrogate
113 modelling and found 34% decrease of system volume and 51.9% decrease of maximum
114 temperature differences. Liao et al.[31] presented optimization of temperature differences for
115 better thermal performance of battery pack using Central Composite Design (CCD) and
116 Response Surface Methods (RSM). Yun et al. [32] designed a framework for simultaneous
117 minimization of battery pack volume and temperature differences using Support Vector

118 Regression (SVR) combined Genetic algorithm approach and the model was optimized using
119 Simulated Annealing (SA). It was found a decrease of 29% in volume and 42% in temperature
120 difference was reported. In brief, these researches focused on the metaheuristics algorithms
121 whose performance is sensitive to choice of settings and often has to be combined with other
122 complex optimization algorithm to optimize it. However, this work illustrates a simpler Finite
123 Element Modelling (FEM) based Automated Neural Network Search (ANS) approach for
124 minimization of temperature related effects and volume of the pack. Settings in ANS approach
125 is selected automatically based on effective search mechanisms.

126 Current study focused more on optimization of design and configuration of battery pack to
127 reduce volume and maximum temperature differences simultaneously. Considering the
128 working conditions of EVs, temperature differences and distribution are important factor which
129 are difficult to optimize [33-35]. Moreover, considering air cooling factors simultaneous
130 optimization of battery pack volume is important to save space in EVs[36]. However, the past
131 literature's hardly considered all these aspects simultaneously for comprehensive optimization
132 of battery pack module. In this context, a comprehensive FEM based ANS approach is
133 proposed. In this proposed approach, firstly the data generated from Finite Element Analysis
134 (FEA) on battery pack module is fed into ANS architecture for generation of models. **The five**
135 **geometric parameters and volume of battery module are considered for model** and the output
136 parameters to be optimized are Maximum temperature differences (TD), Standard deviation of
137 temperature (TSD) and battery pack volume (V). Therefore, motivation of study undertaken is
138 to design an efficient battery pack air cooling system, which optimizes the system volume and
139 cooling performance simultaneously. This paper is structured as follows. Section 2 presents
140 detailed description of the research problem. Section 3 proposes the comprehensive design
141 optimization methodology along with the numerical model. Section 4 provides with results and
142 discussions. In section 5, conclusion is presented.

143 **2 Research problem statement**

144 This section describes the research problem on optimization of operational parameters in air
145 cooling system of battery pack module for obtaining optimal working conditions for EVs
146 shown in Fig.1. A battery pack module containing eight cells is charged and discharged under
147 normal driving conditions as defined in National Renewable Energy Laboratory [37]. Some
148 innovatory ideas were undertaken by assuming the uneven spacing between cells. An uneven
149 gap spacing did not significantly influence the maximum temperature rise of the battery pack
150 module but, it affects the temperature distribution of module. For rigorous investigation, a
151 similar battery module is designed and parameterized, as shown in Fig. 2. The operational
152 parameters are defined as follows:

153 X_1 : Spacing of four cells near the closed end of battery pack module.

154 X_2 : Spacing of four cells near the outlet and inlet for air cooling of battery pack module.

155 X_3 : Spacing in alignment with inlet, between top of the battery cells to the upper board of
156 battery pack module.

157 X_4 : Spacing in alignment with outlet, between top of the battery cells to the lower board of
158 battery pack module.

159 v : Mass flow rate of cooling air in battery pack module.

160 The aim is to analyse the effects of the mentioned five input design parameters on the cooling
161 performance. Based on optimization and subsequent analysis, the findings shall propose a new
162 design of the battery module with better thermal management and minimum volume. For an
163 efficient air cooling of battery module under normal driving conditions, three objectives are
164 thus defined as follows:

165 TD: Maximum temperature differences of eight cells (w.r.t the mean temperature).

166 TSD: Standard deviation of temperature.

167 V: Volume of the battery pack module.

168

169 **Table. 1. Properties of the unit cells used in battery pack model.**

Heat generation rate	28, 000 (W m ⁻³) (1.3 x US06)
Tested drive cycle (aggressive)	600 sec
Power profile	1.3 x US06
Eight Li-ion cells rating	15 Ah
Ambient temperature	27 °C
Active area dimensions	6 x 145 x 255 mm
Specific heat capacity	745 J kg ⁻¹ K ⁻¹
Thermal conductivity	27 W m ⁻¹ K ⁻¹
Density	2335 kg m ⁻³

170

171
$$\text{find } x = [x_1, x_2, x_3, x_4, v]$$

172 minimize V

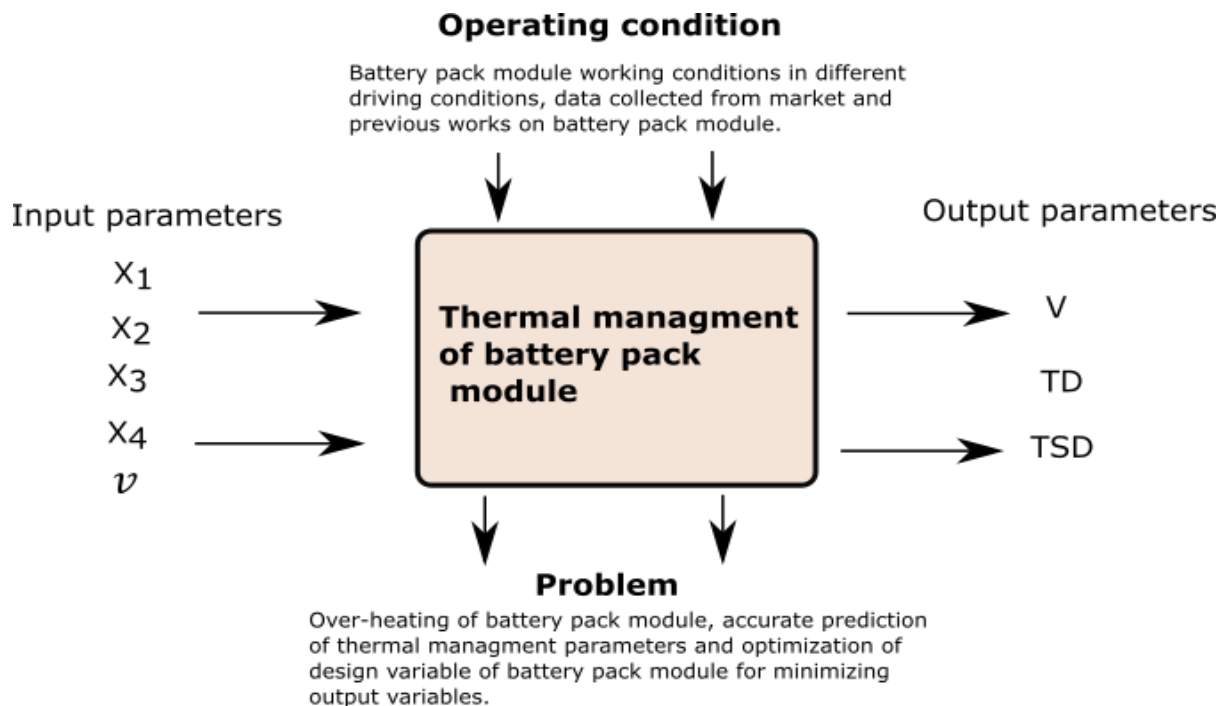
173 minimize TD ... (1.)

174 minimize TSD

175 Such that it follows the constraints of equation 4.

176

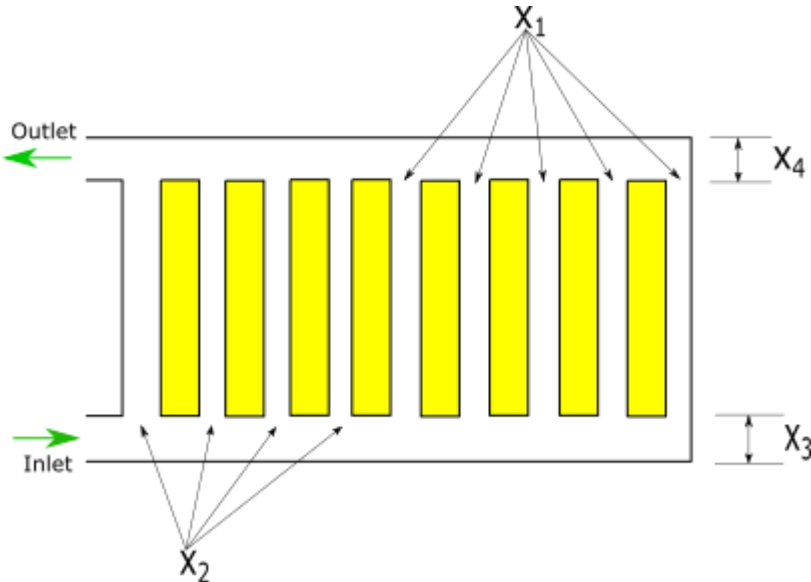
177



178

179
180
181
182
183

Fig. 1 Illustration of research problem statement undertaken.



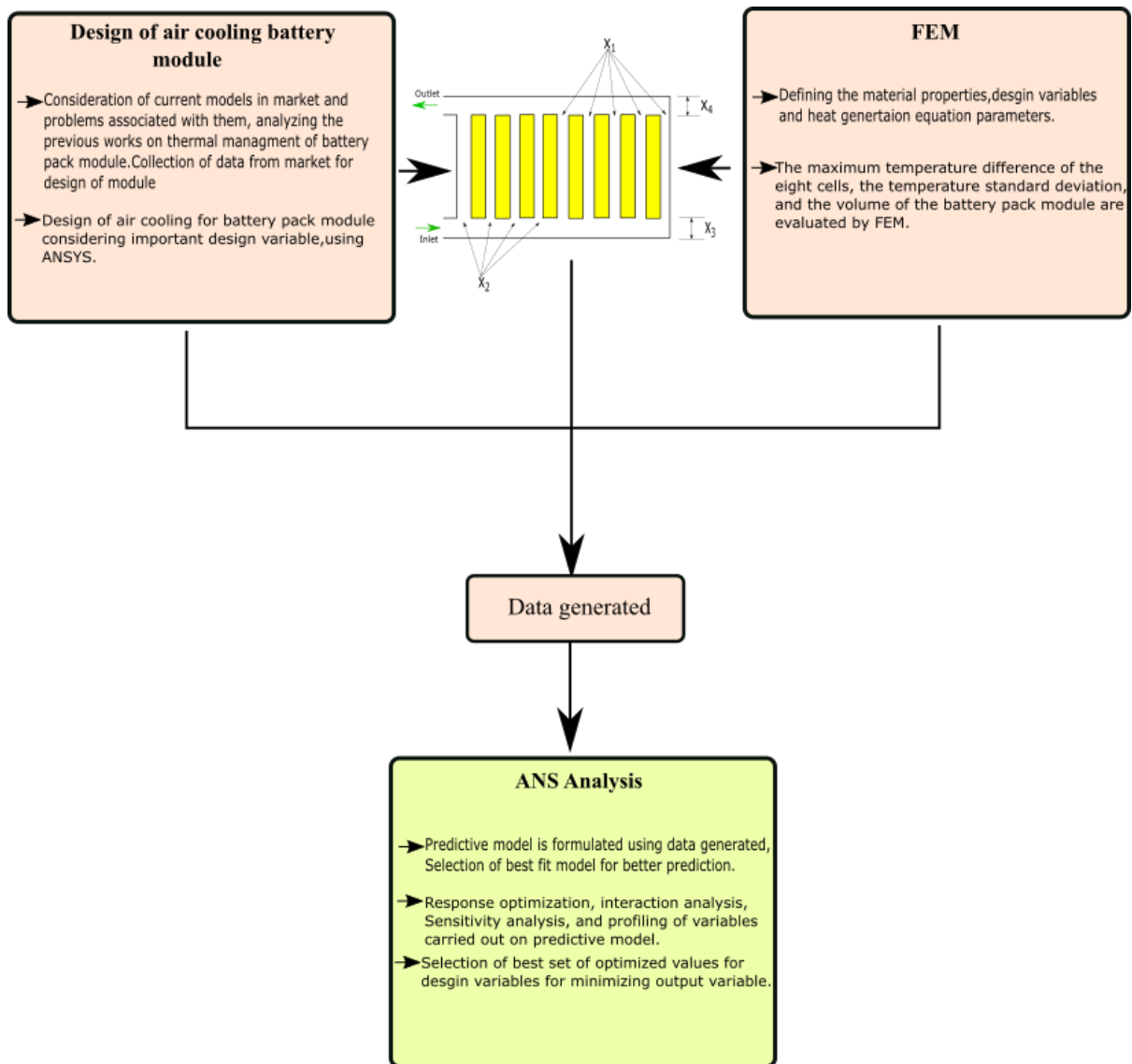
184
185
186
187

Fig. 2 Schematic diagram of battery module with five design variables

188 3 Finite Element Modelling based Automated Neural Network Search approach

189 This section discusses the comprehensive FEM based ANS approach shown in Fig. 3. The
190 approach is illustrated in two subsections 3.1 and 3.2 as follows.

191



192
193

194 **Fig. 3 Finite Element Methodology based Automated Neural Network Search approach**

195

196

197

198 **3.1 Finite Element Method (FEM)**

199 FEM numerical approach is used for modeling thermal behaviour of battery module in EVs.

200 These analysis takes the total area of module and divides it into a finite number of sub-

201 domains/elements. It also uses variation methods to get the solution of the problem by

202 minimizing the error. ANSYS software is used to perform Finite Element Analysis (FEA), it
203 is a widely accepted commercial software package. The knowledge on each of the materials
204 used in the battery module is required for FEM approach to obtain the accurate results.

205 The FEM was applied on battery pack module (Fig. 4) for thermal management. According to
206 working conditions of battery pack, the heat generation of module is set to value of 28,000
207 W/m³, which is 1.3 times normal heat generation conditions [37]. The spatial temperature
208 distribution in each element of the battery pack module is governed by equation 2,

$$209 \quad \frac{\partial^2 T}{\partial x^2} + \frac{\partial^2 T}{\partial y^2} + \frac{\partial^2 T}{\partial z^2} + \frac{\dot{q}_t}{k} = \frac{1}{\alpha} \frac{\partial T}{\partial t} \quad \dots (2)$$

$$210 \quad \dot{q}_t = R_i i^2 - T \Delta S \frac{i}{nF} \quad \dots (3)$$

211 where, x, y and z are spatial directions, k is thermal conductivity (W·m⁻¹·K⁻¹), α = thermal
212 diffusivity (m² s⁻¹). \dot{q}_t is the rate of the internal heat generation per unit volume, R_i is the
213 equivalent resistance of Li-ion cell, i is the discharge current of Li-ion cell per unit volume, F
214 is the Faraday number and ΔS is the entropy change, parameters for \dot{q}_t are referred from
215 equation 3.

216 The results obtained are verified including considerations of fitness function accuracy and
217 mesh independence for the thermal analysis and optimization algorithm. The study aims to
218 demonstrate the effectiveness of non-gradient based optimization in searching for optimum cell
219 arrangement and reveal design principles that can be applied for battery thermal management.

220 After constructing the geometry, meshing, heat generation and governing equations are
221 subsequently applied. In APDL, solid geometry are generally meshed automatically with
222 restraints. For this case, the computational meshes are generated in quadrilateral elements with
223 an edge length of 0.2 cm and maximum aspect ratio of 1.5 for reasonable computing time. As

224 the geometry is altering, the number of elements constructed varies from 5,000 to 10,000.
225 Meshes in the core are refined by increasing the mesh density to achieve higher accuracy in
226 simulating the thermal response.

227

228 Authors have done trial-and-error analysis for investigating mesh influence on performance of
229 model. In order to improve the accuracy in FEM modelling, the number and shape of elements
230 generated are increased and tuned for this particular design. Even the meshes in APDL are
231 created automatically, the size level of elements is further altered to the smallest value by
232 instructing stricter restraints. Ideally, there is not much change in the temperature difference as
233 well as its standard deviation.

234 The air cooling battery module (Fig. 4) is analyzed in ANSYS by incorporating the basic
235 required information as mentioned in [37-38]. The input parameters X_1 , X_2 , X_3 , X_4 and v are
236 varied in battery pack module for the evaluation of maximum temperature difference (TD) of
237 eight cells (w.r.t the mean temperature), Standard deviation of Temperature (TSD) and volume
238 of battery pack module (V). In the present work, the heat generation rate is fixed. All three
239 outputs are dependent on all five input parameters and the input parameters are varied as shown
240 in equation 4. 50 data samples (Table 2) were generated from this process which is then fed
241 into architect of ANS approach for formulation of models for three objective parameters (TD,
242 TSD, V) with respect to the five design variables (X_1 , X_2 , X_3 , X_4 , v). The following section
243 discusses about ANS approach.

244 $1 \text{ mm} \leq x_1 \leq 4 \text{ mm}, 1 \text{ mm} \leq x_2 \leq 4 \text{ mm}, 1 \text{ mm} \leq x_3 \leq 4 \text{ mm}, 1 \text{ mm} \leq x_4 \leq 4 \text{ mm}$

245 $0.002 \text{ Kg} / s \leq v \leq 0.02 \text{ Kg} / s \quad \dots(4)$

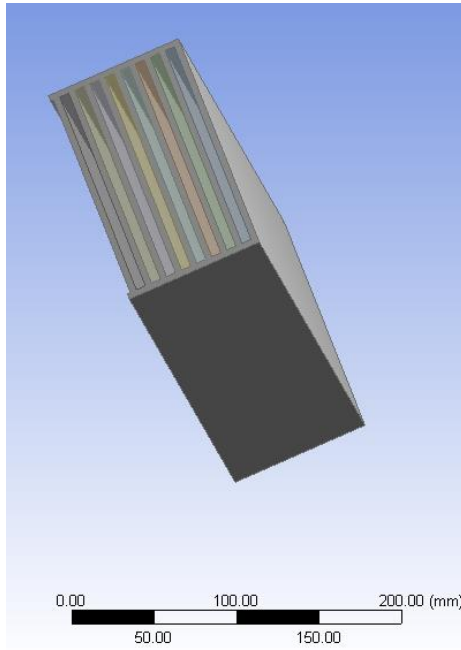


Fig. 4 Computational region of battery module for air cooling.

246
247

248

249

Table 2. Data generated from thermal modelling of battery pack using FEM

Run no.	Input parameters					Output parameters		
	X1 (mm)	X2 (mm)	X3 (mm)	X4 (mm)	v (kg/s)	V (m ³)	TD (K)	TSD (K)
1	2.11	1.81	3.73	1.21	0.00974	0.002518	8.57999	4.93789
2	1.39	3.55	1.45	2.89	0.01478	0.002636	5.02078	1.11791
3	2.23	1.09	1.27	2.11	0.0119	0.002405	5.09854	1.71818
4	1.33	2.29	2.11	1.03	0.01262	0.002412	9.9375	5.1425
5	1.93	2.65	1.33	1.87	0.0191	0.002581	4.45999	0.954862
6	3.49	3.85	2.35	3.43	0.0101	0.003112	7.56027	2.06045
7	1.87	2.11	3.97	3.37	0.01442	0.002559	5.32123	2.1044
8	3.61	3.31	3.49	2.77	0.00578	0.003062	9.5433	5.13151
9	3.43	2.35	1.21	1.63	0.01622	0.002812	5.95364	3.40527
10	2.71	3.67	3.43	2.53	0.01802	0.002938	8.49246	4.27937
11	1.45	3.25	1.39	1.57	0.00758	0.002577	7.05188	2.90261
12	3.25	3.43	1.99	2.23	0.00218	0.002969	9.9736	3.73074
13	1.63	3.73	3.01	3.61	0.01082	0.002751	6.89923	2.86642
14	2.89	2.77	2.05	3.85	0.00362	0.002832	8.20624	2.39122
15	3.07	1.39	2.59	3.91	0.01334	0.002665	5.30655	1.25034
16	1.81	3.37	3.13	3.07	0.0029	0.002723	9.8786	4.67427
17	1.51	1.45	2.17	1.69	0.00434	0.002331	8.08087	3.81214
18	2.35	2.53	1.15	3.79	0.01118	0.002674	6.44733	2.0034

19	2.77	1.63	3.25	2.17	0.00254	0.002625	9.44736	4.16184
20	3.31	1.51	3.91	2.35	0.01154	0.002726	7.00259	4.73956
21	2.65	1.57	1.63	3.25	0.01874	0.002583	4.67157	0.943342
22	3.67	2.95	1.09	2.95	0.01226	0.002972	8.47672	2.42016
23	2.29	3.91	1.51	2.83	0.00722	0.002862	6.71506	2.24993
24	2.05	3.01	2.83	1.27	0.00326	0.002675	10.5788	5.3401
25	2.95	3.49	1.81	2.65	0.01982	0.002926	5.33734	0.989422
26	3.37	3.07	1.75	1.15	0.00902	0.00291	8.75858	4.42346
27	1.15	3.61	2.95	1.81	0.01046	0.002607	9.96359	5.38074
28	3.55	2.59	3.37	1.39	0.00686	0.002909	9.69901	5.06779
29	1.69	2.47	2.47	3.97	0.01586	0.002565	4.52307	0.975731
30	1.75	1.27	2.71	1.75	0.01694	0.002359	5.04529	3.43288
31	3.85	1.33	2.41	2.41	0.01514	0.002775	4.99002	1.77981
32	3.79	2.71	2.53	3.49	0.01766	0.002999	5.35361	0.823158
33	2.83	1.21	1.69	3.31	0.00614	0.002565	7.46188	3.24942
34	2.17	1.93	3.61	3.67	0.00506	0.002589	7.10147	2.54214
35	3.73	1.75	3.19	3.55	0.0065	0.002853	6.66385	2.38894
36	2.47	3.79	3.85	2.05	0.00866	0.002909	9.95065	5.23092
37	2.53	3.97	2.29	1.45	0.01406	0.002905	9.64435	4.64936
38	1.57	1.03	2.77	3.13	0.00938	0.002311	5.05328	1.41773
39	1.03	2.17	3.55	2.29	0.00794	0.002381	8.4606	4.81907
40	2.59	1.69	3.31	2.71	0.01946	0.002611	4.97839	3.19006
41	3.01	3.13	3.67	3.73	0.01298	0.002941	6.77084	3.98288
42	3.19	1.15	2.23	1.33	0.0083	0.002599	7.51358	4.89955
43	2.41	2.23	1.03	1.99	0.0047	0.002605	7.53839	2.22204
44	1.99	2.83	3.79	1.51	0.01658	0.002658	8.63937	4.70958
45	1.09	1.87	1.57	3.01	0.0137	0.002326	4.16092	1.22898
46	1.21	2.89	2.89	2.59	0.01838	0.00252	6.7894	3.75226
47	3.13	2.05	2.65	1.09	0.0173	0.002727	9.17682	5.27326
48	3.97	3.19	3.07	1.93	0.0155	0.003086	7.11981	3.5573
49	3.91	1.99	1.87	2.47	0.00542	0.002878	7.23776	2.36477
50	1.27	2.41	1.93	3.19	0.00398	0.002452	8.16791	3.25939

251

252

253

254 **3.2 Automated Neural Network Search approach**

255 ANS is an machine learning method used for predictive modelling of complex systems. The
 256 principle of ANS is same as Artificial Neural Network (ANN), except the activation function
 257 and training algorithm selection is automated. The ANS model can optimize its response by

258 adjusting it according to the feedback it receives. The network/architecture of such model is
259 shown in Fig. 5. When the network is implemented, the input variable values are placed in the
260 input units, the hidden and output layer units are gradually executed in their serial order
261 triggered by activation functions and trained on the basis of errors. Random weight
262 initialization is preferred option for this particular analysis as the activation function and
263 training algorithm is automated. It is found that generally, the two layer neural network with
264 tan-sigmoid activation/threshold functions at hidden layer and pure linear activation function
265 at output layer can train for any set of non-linear data [39]. Output parameters are affected by
266 a great variety of interaction between input parameters. It is very difficult to illustrate their
267 relationship by the use of conventional methods. Therefore, ANS is preferred tool in this
268 perspective. The ANS facility is used for formulating the neural networks with various
269 configurations and settings while requiring nominal specifications. It forms number of
270 networks models with algorithmic combinations. The network which achieve the highest
271 correlation coefficient value between targets and outputs of the network is chosen. In ANS,
272 there are mainly two types of networks, Multilayer Perceptron (MLP) network type and Radial
273 Basis Function (RBF) network. In present work, we choose MLP as network type because the
274 problem is multi-dimensional and multi-objective in nature [39]. The STATISTICA 12
275 software package is used to implement this MLP network.

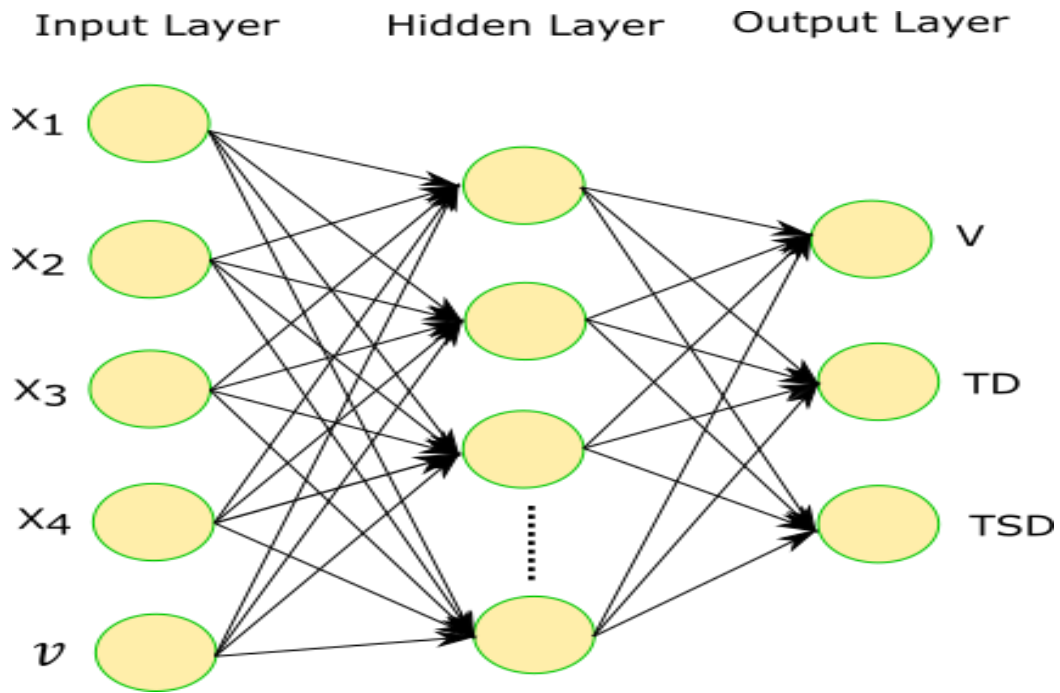


Fig. 5 Illustration of Artificial Neural Network Search (ANS)

276

277

278

279 The data generated from FEM is divided into three different sets comprising of training, testing

280 and validation. The training data is set to 75%, test data to 15% and validation data to 10%.

281 The sampling of data is done randomly. Networks to train is set to 2000 and 10 best

282 performance coefficient networks are retained. The ANS models are selected on basis of there

283 performance coefficient values (Table 5). The ANS models with high performance coefficient

284 and simultaneously having low error values, are accurate and stable for optimization. The value

285 of seed for sampling is 1000. After training, we retain 8 networks which are best suited for

286 predictive modelling for 3 outputs. Two models were formulated for 3 output variables.

287 Settings used for $V(m^3)$, and TSD (K) is shown in table 3 and settings used for TD (K) is shown

288 in table 4. The networks are trained and tested on FEM generated data for thermal management

289 of battery pack module. Fig. 3 shows the flowchart illustration of methodology undertaken.

290 The main objective for network generation is to formulate a robust and an accurate predictive

291 model. Further, optimization of these model results in optimum values of five design variables
 292 (X_1, X_2, X_3, X_4, v) that simultaneously optimizes the three outputs (TD, TSD, V).

293
 294

295 **Table 3. Settings of the Automated neural network search for V and TSD outputs.**

Settings	Values
Multilayer Perceptron (MLP)	Min hidden units =10, Maximum hidden units = 10
Radial Basis Function (RBF)	Min hidden units =0, Maximum hidden units = 0
Networks to train	2000
Networks to retain	10
Type of activation functions used for hidden and output neurons	Identity, logistic

296
 297

298 **Table 4. Settings of the Automated neural network search for TD output.**

Settings	Values
Multilayer Perceptron (MLP)	Min hidden units =4, Maximum hidden units = 4
Radial Basis Function (RBF)	Min hidden units =0, Maximum hidden units = 0
Networks to train	2000
Networks to retain	10
Type of activation functions used for hidden and output neurons	Identity, logistic, Tanh, Exponential, Sine

299
 300

301 **4 Results and Discussion**

302 **4.1 Statistical fit of Automated Neural Network Search models**

303 Table 5 shows the 50 runs for the network generated, the performance (correlation coefficient)
 304 of the given networks on the training, testing, and validation data, training algorithm and the
 305 activation function for the hidden and output neurons. Only the fewer ANS models (highlighted
 306 in Table 5) with the training correlation coefficient higher than 0.955 are chosen as the best
 307 networks (Table 6). The model chosen for analysis are model no. 23 and 47 (highlighted red in

308 Table 6), where model no. 23 (MLP 5-10-3) is used for analysis of V and TSD, and model no.
309 47 (MLP 5-4-1) is used for analysis of TD. Fig. 6 describes the fitting of models for all output
310 parameters. The coefficient of determination values are found to be 0.99, 0.94 and 0.86 for V,
311 TD and TSD respectively. Fig. 6 (a), (b) and (c) illustrates line fit plot for three outputs V, TD
312 and TSD respectively. Fig. 7, explains that the input parameters X_4 and X_3 are the most
313 dominant ones for influencing outputs (V and TSD) for model no.23, whereas for model no.
314 47, X_4 and v are the most dominant input parameters for influencing (TD). Overall, the main
315 influencing input parameters are X_4 , v and X_3 for three response variables V, TD and TSD.

316 **Table 5. 50 generated models of Automated Neural Network Search**

Index	Network name	Training Perf.	Test Perf.	Validation Perf.	Training algorithm	Hidden activation	Output activation
1	MLP 5-8-3	0.950015	0.884071	0.990848	BFGS 38	Logistic	Identity
2	MLP 5-8-3	0.947831	0.881299	0.990640	BFGS 31	Logistic	Identity
3	MLP 5-8-3	0.948579	0.881561	0.993897	BFGS 29	Logistic	Identity
4	MLP 5-8-3	0.953264	0.883503	0.997169	BFGS 36	Logistic	Identity
5	MLP 5-8-3	0.948555	0.852924	0.990801	BFGS 25	Logistic	Identity
6	MLP 5-8-3	0.949140	0.887160	0.990776	BFGS 37	Logistic	Identity
7	MLP 5-8-3	0.949538	0.880357	0.992928	BFGS 29	Logistic	Identity
8	MLP 5-8-3	0.949767	0.870302	0.992069	BFGS 33	Logistic	Identity
9	MLP 5-8-3	0.948773	0.876464	0.991214	BFGS 30	Logistic	Identity
10	MLP 5-8-3	0.956261	0.872637	0.992882	BFGS 40	Logistic	Identity
11	MLP 5-9-3	0.950602	0.898850	0.991570	BFGS 27	Logistic	Identity
12	MLP 5-9-3	0.954556	0.887046	0.991808	BFGS 37	Logistic	Identity
13	MLP 5-9-3	0.952105	0.876715	0.994322	BFGS 36	Logistic	Identity
14	MLP 5-9-3	0.953413	0.880951	0.991649	BFGS 33	Logistic	Identity
15	MLP 5-9-3	0.952844	0.885069	0.993374	BFGS 39	Logistic	Identity
16	MLP 5-9-3	0.951527	0.891649	0.992997	BFGS 40	Logistic	Identity
17	MLP 5-9-3	0.950306	0.873274	0.992540	BFGS 35	Logistic	Identity

18	MLP 5-9-3	0.951601	0.864137	0.991732	BFGS 36	Logistic	Identity
19	MLP 5-9-3	0.947856	0.885238	0.991718	BFGS 35	Logistic	Identity
20	MLP 5-9-3	0.952937	0.880276	0.994892	BFGS 42	Logistic	Identity
21	MLP 5-10-3	0.948406	0.858631	0.991307	BFGS 27	Logistic	Identity
22	MLP 5-10-3	0.951390	0.881621	0.990769	BFGS 33	Logistic	Identity
23	MLP 5-10-3	0.968015	0.872972	0.992018	BFGS 43	Logistic	Identity
24	MLP 5-10-3	0.949296	0.877779	0.991130	BFGS 26	Logistic	Identity
25	MLP 5-10-3	0.955552	0.863405	0.992462	BFGS 37	Logistic	Identity
26	MLP 5-10-3	0.947882	0.893928	0.991056	BFGS 27	Logistic	Identity
27	MLP 5-10-3	0.954687	0.867890	0.992050	BFGS 23	Logistic	Identity
28	MLP 5-10-3	0.947397	0.871344	0.992350	BFGS 25	Logistic	Identity
29	MLP 5-10-3	0.951077	0.867050	0.993351	BFGS 33	Logistic	Identity
30	MLP 5-10-3	0.949470	0.874669	0.990985	BFGS 26	Logistic	Identity
31	MLP 5-7-1	0.882770	0.775362	0.923379	BFGS 3	Identity	Logistic
32	MLP 5-7-1	0.954002	0.918905	0.924436	BFGS 19	Logistic	Exponential
33	MLP 5-11-1	0.848846	0.832199	0.925970	BFGS 4	Identity	Tanh
34	MLP 5-4-1	0.963519	0.906612	0.965862	BFGS 39	Logistic	Tanh
35	MLP 5-10-1	0.894180	0.752153	0.935306	BFGS 9	Tanh	Exponential
36	MLP 5-4-1	0.943157	0.893595	0.994154	BFGS 24	Logistic	Tanh
37	MLP 5-4-1	0.925115	0.795487	0.989075	BFGS 18	Exponential	Identity
38	MLP 5-4-1	0.945285	0.804359	0.988869	BFGS 24	Logistic	Logistic
39	MLP 5-4-1	0.969057	0.921703	0.994828	BFGS 41	Logistic	Identity
40	MLP 5-4-1	0.971912	0.891941	0.992240	BFGS 31	Tanh	Logistic
41	MLP 5-4-1	0.951497	0.828912	0.994789	BFGS 25	Logistic	Identity
42	MLP 5-4-1	0.935016	0.817722	0.991961	BFGS 23	Logistic	Identity
43	MLP 5-4-1	0.939505	0.850236	0.990311	BFGS 22	Logistic	Identity
44	MLP 5-4-1	0.937383	0.792258	0.991671	BFGS 20	Logistic	Identity
45	MLP 5-4-1	0.931978	0.835205	0.988943	BFGS 24	Logistic	Identity
46	MLP 5-4-1	0.933245	0.761554	0.997105	BFGS 19	Logistic	Identity

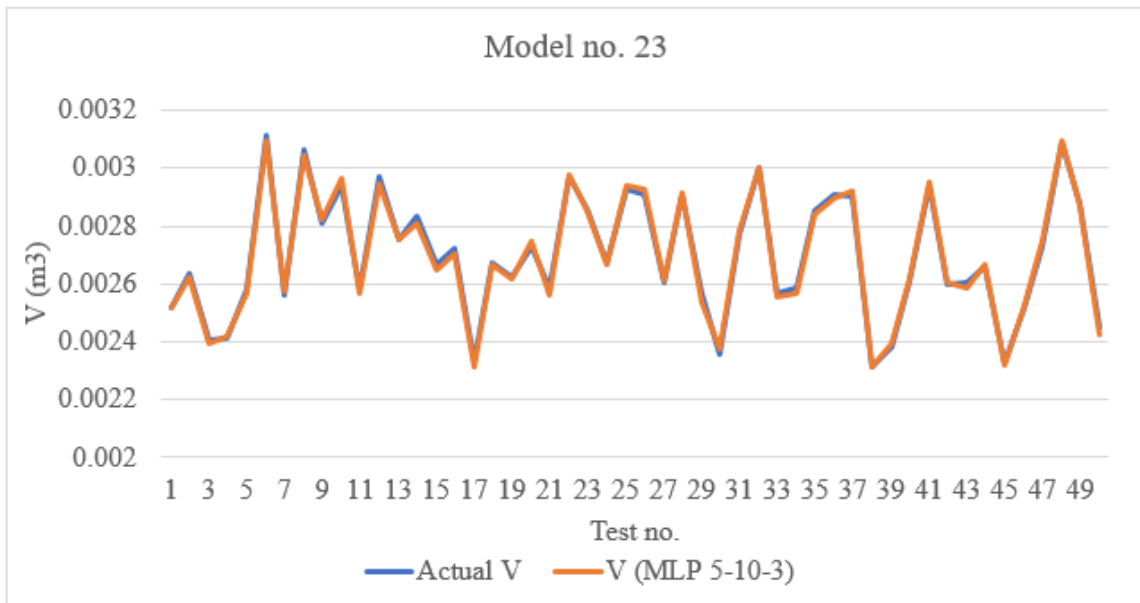
47	MLP 5-4-1	0.985318	0.833880	0.993047	BFGS 26	Tanh	Exponential
48	MLP 5-5-1	0.975114	0.819712	0.997844	BFGS 23	Tanh	Exponential
49	MLP 5-4-1	0.962713	0.853720	0.998900	BFGS 16	Logistic	Tanh
50	MLP 5-5-1	0.970930	0.923706	0.995444	BFGS 33	Tanh	Logistic

317
318
319
320
321

Table 6. Best fit ANS models networks

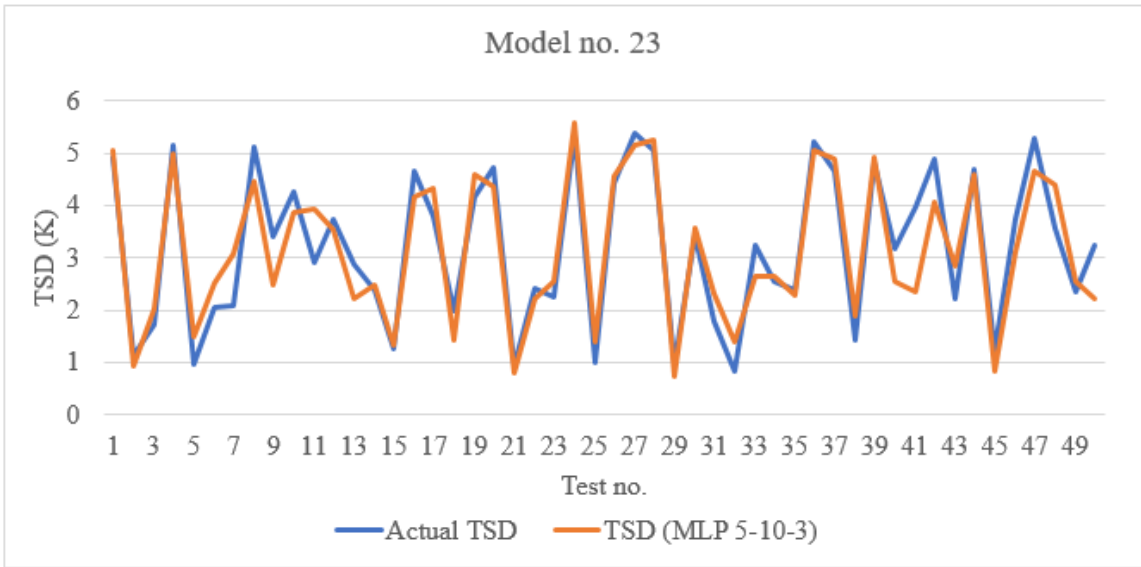
Index	Network name	Training Perf.	Test Perf.	Validation Perf.	Training algorithm	Hidden activation	Output activation
10	MLP 5-8-3	0.956261	0.872637	0.992882	BFGS 40	Logistic	Identity
23	MLP 5-10-3	0.968015	0.872972	0.992018	BFGS 43	Logistic	Identity
25	MLP 5-10-3	0.955552	0.863405	0.992462	BFGS 37	Logistic	Identity
27	MLP 5-10-3	0.954687	0.867890	0.992050	BFGS 23	Logistic	Identity
47	MLP 5-4-1	0.985318	0.833880	0.993047	BFGS 26	Tanh	Exponential
48	MLP 5-5-1	0.975114	0.819712	0.997844	BFGS 23	Tanh	Exponential
49	MLP 5-4-1	0.962713	0.853720	0.998900	BFGS 16	Logistic	Tanh
50	MLP 5-5-1	0.970930	0.923706	0.995444	BFGS 33	Tanh	Logistic

322
323
324
325



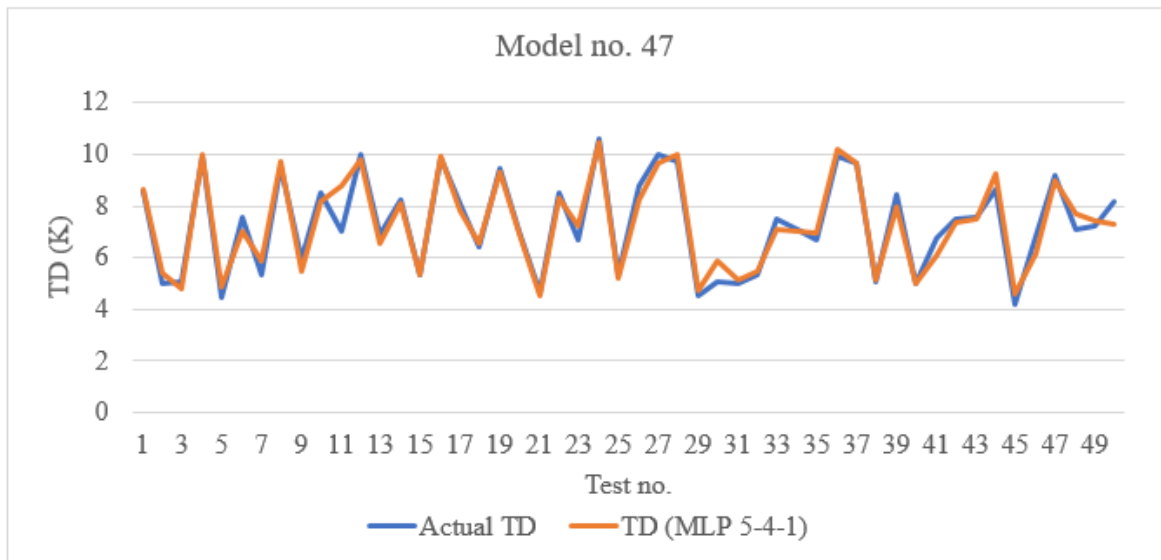
326
327

(a.)



328
329

(b)



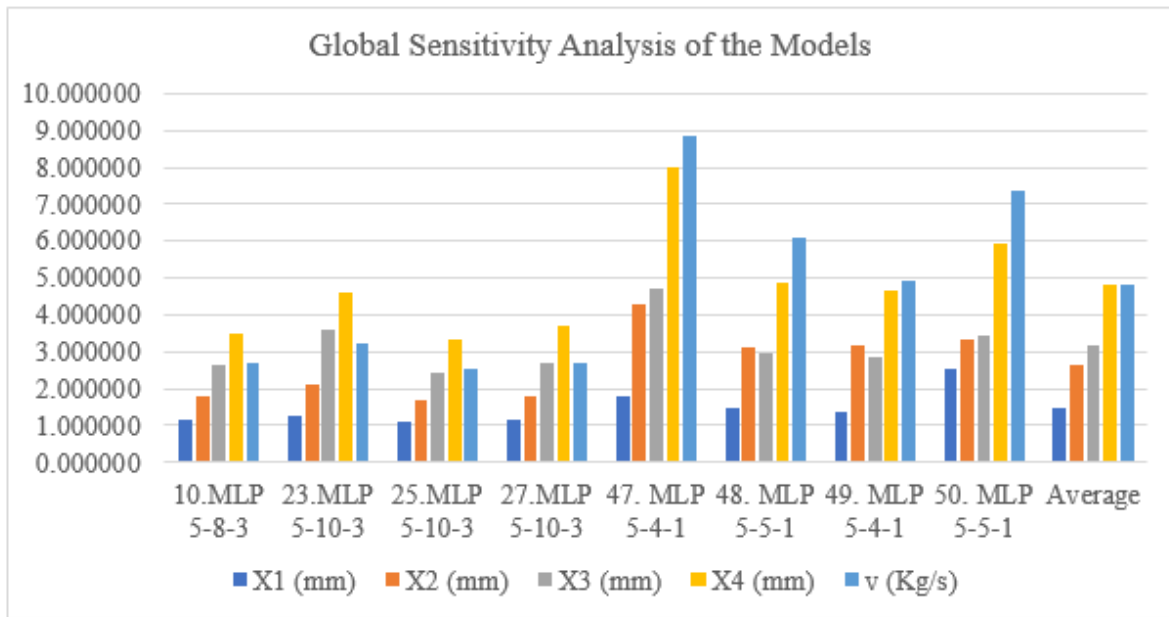
330
331

(c)

Fig. 6 Line fit plot of Actual and ANS models for the three outputs

332
333
334

335



336

337

Fig. 7 Global sensitivity analysis for the selected models showing the importance of individual input parameters on the three outputs

338

339

340

341

342

343 4.2 Response optimization of selected Automated Neural Network Search models

344 Response optimization is performed on selected ANS models 23 and 47 for simultaneously

345 minimizing volume of battery module, Temperature difference and Temperature standard

346 deviation. **Non-dominated sorting genetic algorithm II (NSGA II ANSYS software package)**

347 combined with simplex and grid search is used for optimization. Number of iterations was set

348 to 1000 and number of initial samples was set to 100. The selected models were evaluated to

349 obtain the minimum volume of battery module, Temperature difference and standard deviation

350 of temperature. **The initial values of gap spacing X_1 , X_2 , X_3 , and X_4 are set to 4 mm and v is set**

351 **to 0.012 kg/s. The value of v is fixed, it is not varied only the values of geometric parameters**

352 **are varied.** Step size is set to 0.0874 and 0.00052 for (X_1 , X_2 , X_3 , X_4) and v respectively, and

353 the operating range of design variables were set from 1 mm to 4 mm and 0.002Kg/s to 0.02Kg/s

354 for (X_1 , X_2 , X_3 , X_4) and v respectively. Given these set of input values, the initial values

355 obtained from ANS models for V, TD and TSD are 0.003279m³, 6.813K and 4.37K
356 respectively. The multi-objective optimized result is given in Table 7. The volume of the
357 battery pack module reduces from 0.0033m³ to 0.0023m³ by 29.21%, the maximum
358 temperature difference of the eight cells reduces from 6.81K to 4.38K by 35.66%, and the
359 standard deviation of temperature reduces from 4.38K to 0.93K by 78.69%. Fig. 8 shows the
360 iterations graph of simplex search for optimization of three response variables. The
361 optimization objective is met w.r.t above optimization constraints and the results obtained on
362 improvement are feasible. The decrease in the volume of battery module after optimization
363 decreases the cost of manufacturing of battery pack. The reduction of TSD by 78.69% enables
364 the uniformity of temperature in different parts of battery module. Due to reduction of
365 maximum temperature differences by 35.66% the battery life is maintained in long run and
366 working conditions.

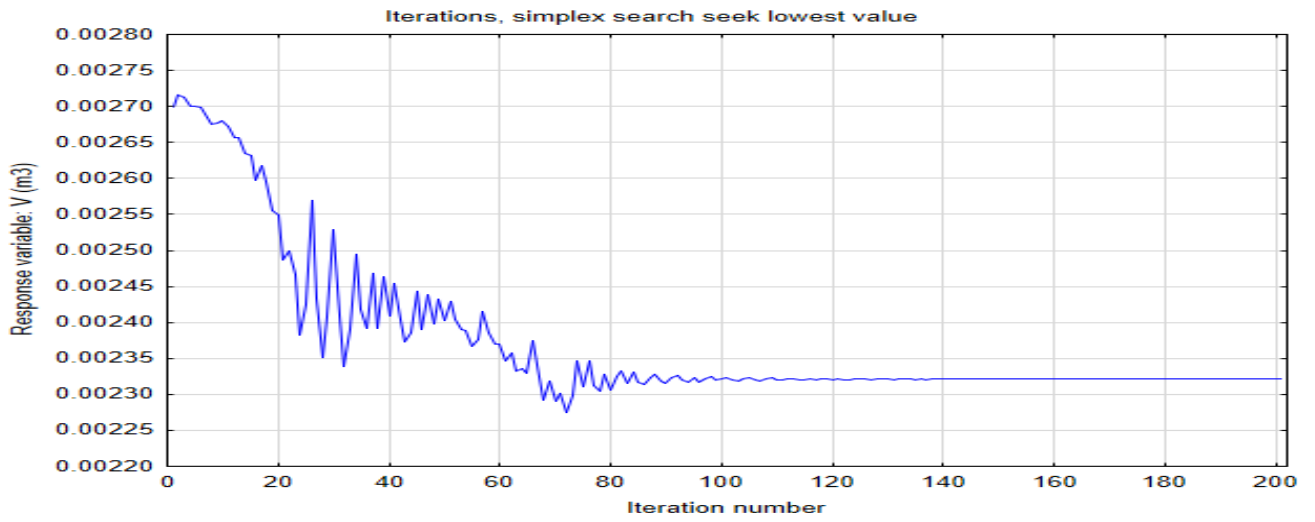
367

368 **Table 7. Multi-objective optimization results for the battery module**

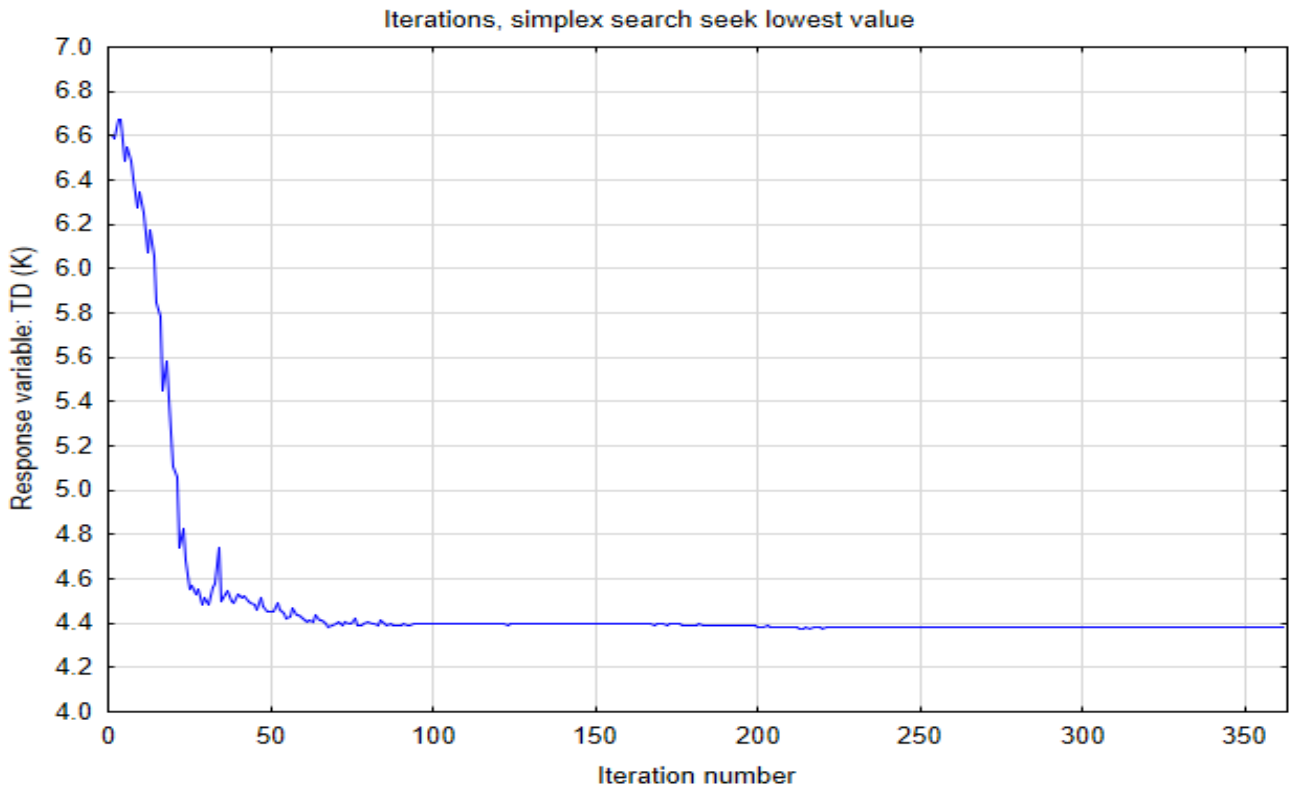
	Design variables					Objective variables		
	X1(mm)	X2(mm)	X3(mm)	X4(mm)	v (Kg/s)	V (m3)	TD (K)	TSD (K)
Initial values	4	4	4	4	0.012	0.003279	6.813343	4.379044
Range/ constraint	[1, 4]	[1, 4]	[1, 4]	[1, 4]	[0.002, 0.02]	minimize	minimize	minimize
Optimum values	1.422795	1.418067	1.698304	2.894863	0.019353	0.002321	4.383997	0.933274
%Improvement in Objective						+29.21%	+35.66%	+78.69%

369

370



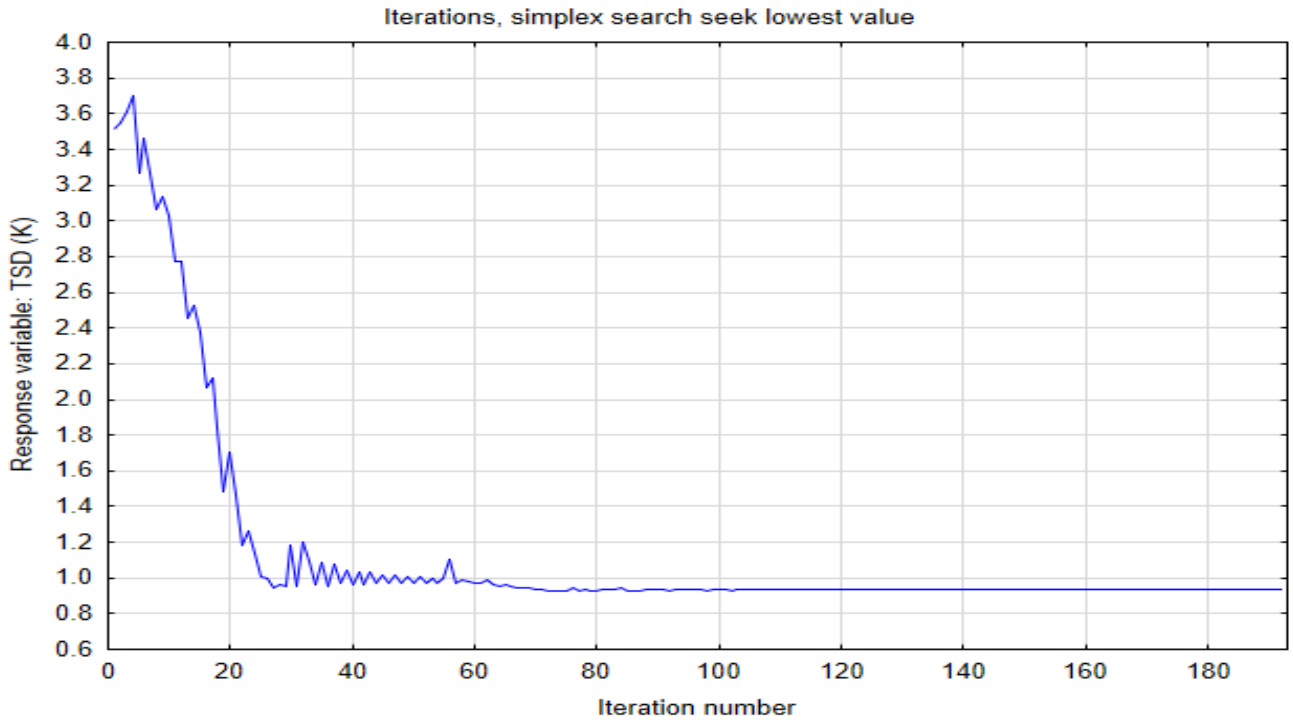
(a.)



(b.)

371
372
373
374

375
376
377
378



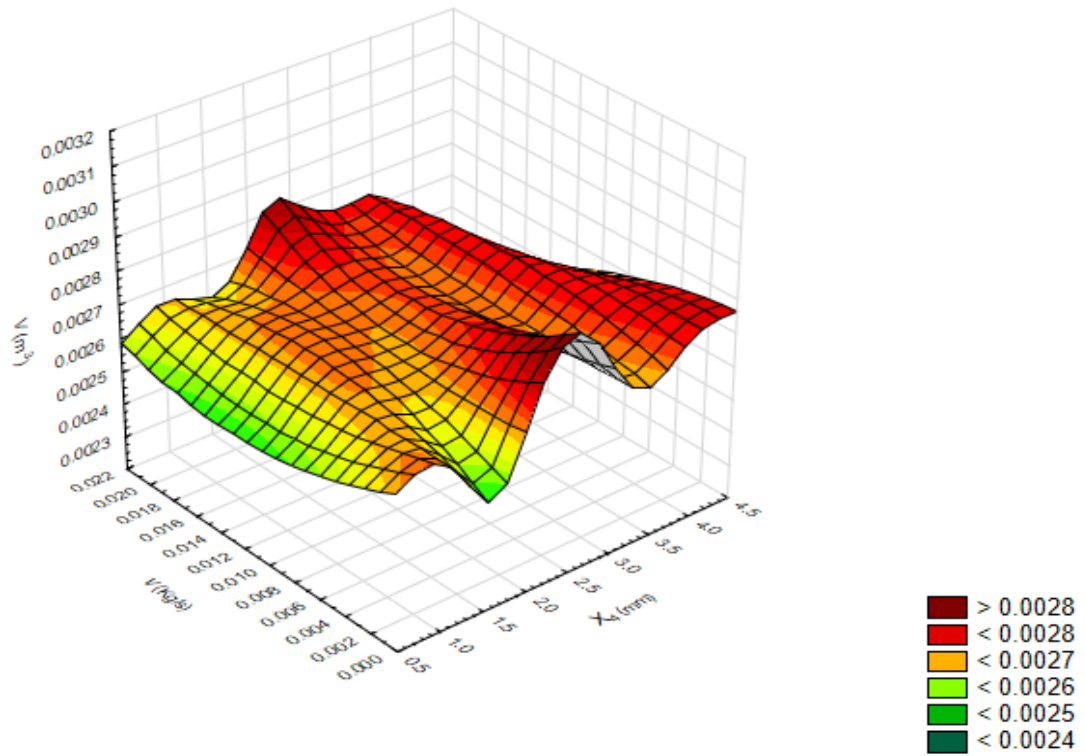
(c.)

Fig. 8 Optimization results for determination of minimum value of V, TD and TSD

4.3 3-D surface plots and Simulation distribution for robustness validation

3-D graphs are plotted between the response variable and the most influencing design variables determined by global sensitivity analysis. 3-D surface plots and sequential plots are used to study the variations of response variable due to interactions between the two or more-design variable. The nature or trend of variations in response variable is studied w.r.t variations in design variables. Fig. 9 shows the 3D surface plots of the V, TD and TSD w.r.t X_4 and v design variables. 3-D sequential plots (Fig. 10), shows the plot of design variable and response variables, which describes the variation of all variables over whole range of run.

3D Surface Plot of V (m^3) against X_4 (mm) and V (Kg/s)



395

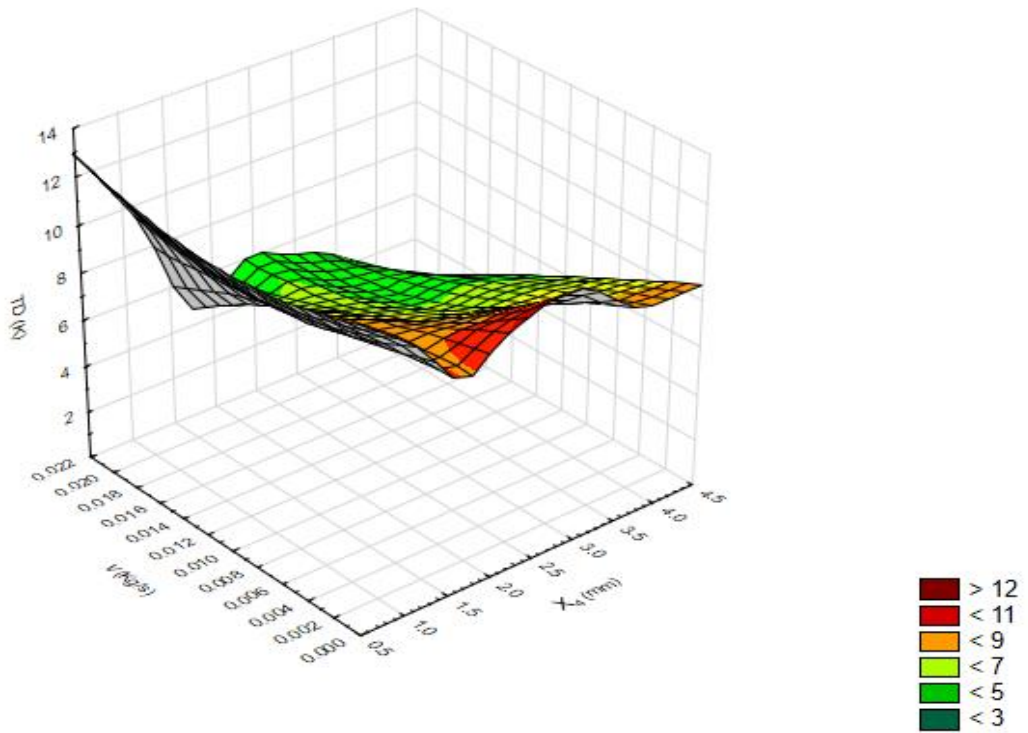
(a.)

396

397

398

3D Surface Plot of TD (K) against X_4 (mm) and V (Kg/s)

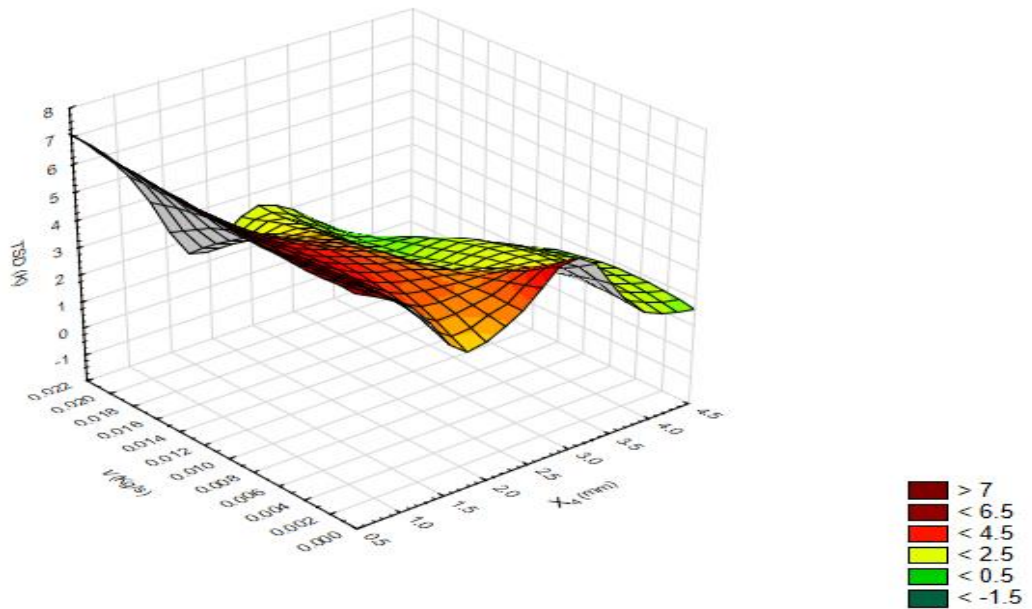


399

(b.)

400

3D Surface Plot of TSD (K) against X_4 (mm) and V (Kg/s)



401

(c.)

402

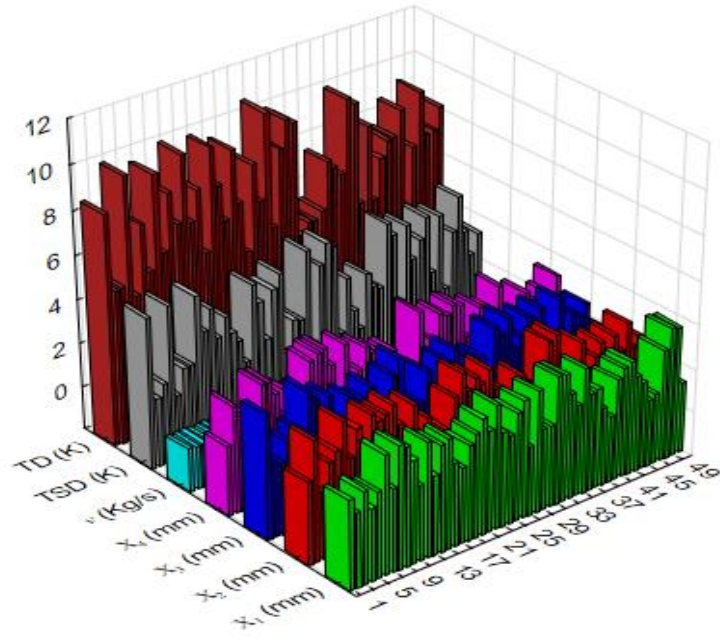
403

Fig. 9 3-D surface plots showing variations of response variable w.r.t influencing design variables

404

405

3D Sequential Graph for X1, X2, X3, X4, v, TD and TSD.



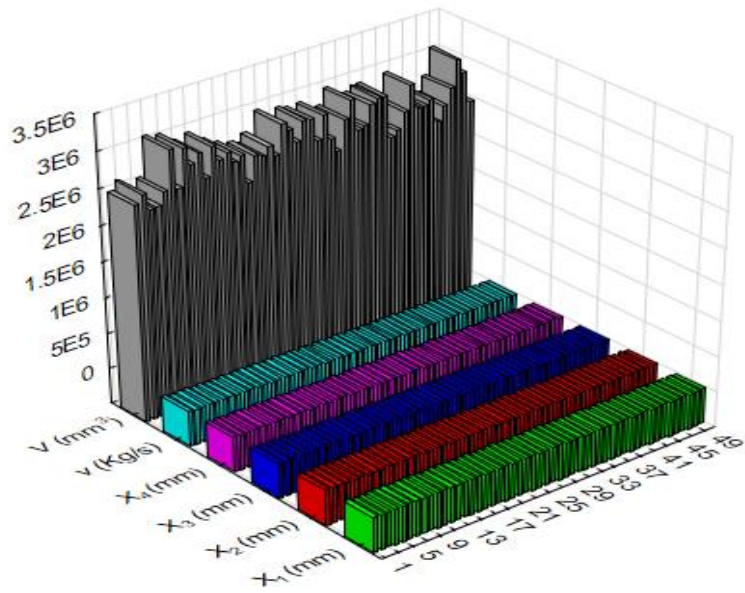
406

407

(a.)

408

3D Sequential Graph for X1, X2, X3, X4, v and V.



409

410

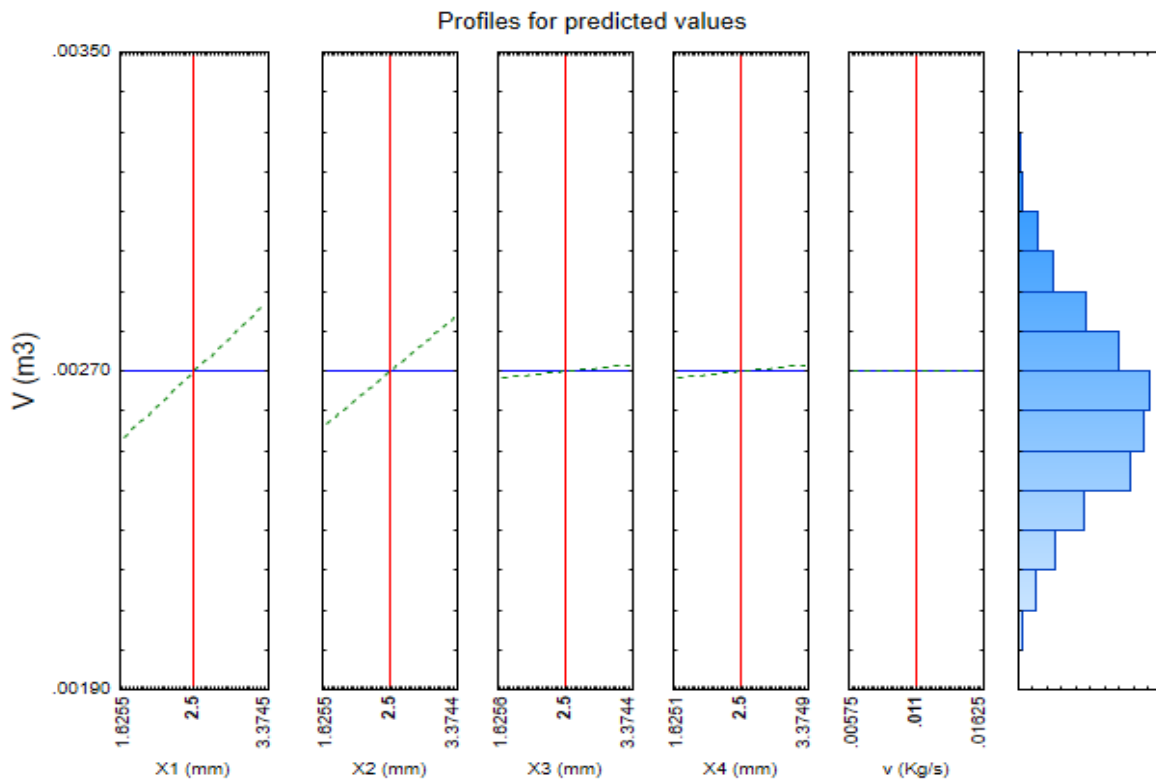
(b.)

411

Fig. 10 3D sequential plot showing variation of all variables over whole range of run

412 Profiling of the ANS model is done to understand the desirability of response variables (V, TD
 413 and TSD) for different levels of individual input variables in their individual specified range.
 414 Level of input variables which best fit with the desirability of the response variable is selected
 415 as the set of conditions for design. Profiling of predicted values for individual response
 416 variables (V, TD and TSD) are shown in Fig. 11. In Fig. 11 (a.) for response variable V it is
 417 observed that v(Kg/s) design variable is constant over range of V, while other variables are
 418 having linear variations and distribution is not reflecting any sudden changes. As shown in Fig.
 419 11 (b.), the response variable TD is also having normal distribution. The mean value of
 420 response variable TD is in range 4 K to 7.3099 K. Fig. 11 (c.) shows the skewness in
 421 distribution of TSD for region above 3.217 K.

422

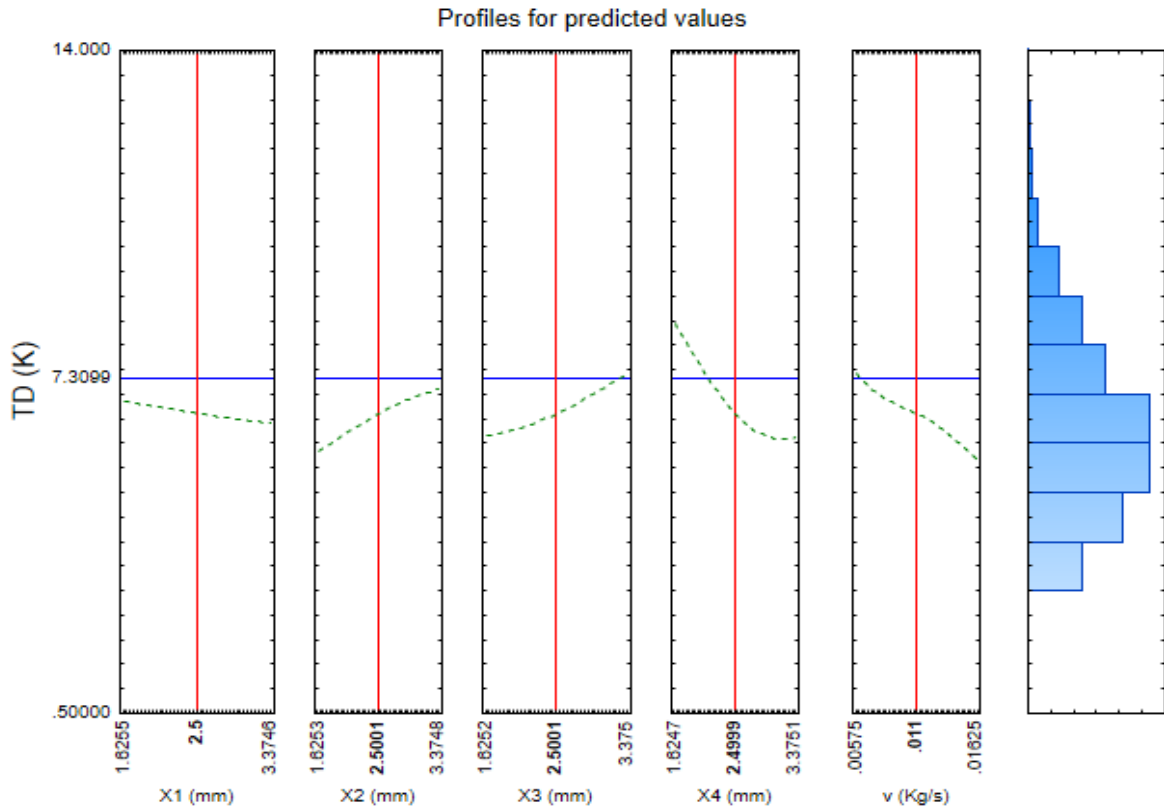


423

424

(a.)

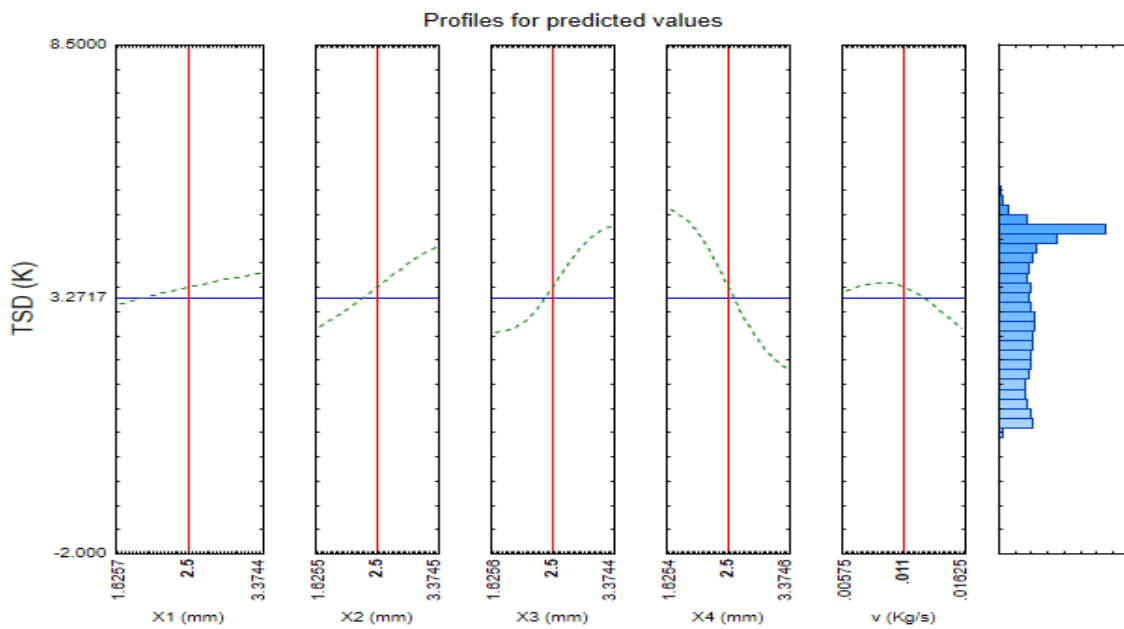
425



426

427

(b.)



428

429

(c.)

430 **Fig. 11 Profiling normal distribution of individual response variables on different levels**
 431 **of input variables.**

432 **5 Conclusions**

433 In the current study, the research problem on optimization of design variables of battery module
434 to minimize response variables (Maximum temperature differences, standard deviation of
435 temperature over region of battery pack module and volume of battery pack) for air-cooling
436 thermal management of battery module is undertaken. To solve this problem, a comprehensive
437 FEM based ANS approach is proposed. The methodology is applied on the battery module
438 comprising of eight prismatic cells. The optimized air-cooled battery pack module have better
439 thermal performance in normal working conditions of EVs compared to initial designed
440 scheme. The main findings from the analysis and optimization performed are as follows:

441 (1) The volume of the battery pack module decreases from 0.003279 m^3 to 0.002321 m^3 by
442 29.21% which addresses the space consumption in EVs and favors economical factors.
443 The maximum temperature differences of the eight cells decreases from 6.81 K to 4.38
444 K by 35.66% and the temperature standard deviation reduces from 4.38 K to 0.93 K by
445 78.69%.

446 (2) The optimized air-cooled battery pack module has lesser volume consumption. This
447 implies, it exhibits lower maximum temperature differences in battery module and the
448 uniformity in temperature distribution over battery module is attained.

449 The present work provides an empirical and feasible model for design of battery thermal
450 management system. This analysis can be scaled-up to battery packs comprising of 100 or more
451 cells as in case of energy storage systems and commercial EVs.

452 **Acknowledgement**

453 Authors like to acknowledge Grant DMETKF2018019 by State Key Lab of Digital Manufacturing
454 Equipment & Technology (Huazhong University of Science and Technology).

455

456

457 **References**

- 458 [1] Masayoshi, W. A. D. A. (2009). Research and development of electric vehicles for clean
459 transportation. *Journal of Environmental Sciences*, 21(6), 745-749.
- 460 [2] Skerlos, S. J., & Winebrake, J. J. (2010). Targeting plug-in hybrid electric vehicle policies to
461 increase social benefits. *Energy Policy*, 38(2), 705-708.
- 462 [3] Avadikyan, A., & Llerena, P. (2010). A real options reasoning approach to hybrid vehicle
463 investments. *Technological Forecasting and Social Change*, 77(4), 649-661.
- 464 [4] Peterson, S. B., Whitacre, J. F., & Apt, J. (2010). The economics of using plug-in hybrid electric
465 vehicle battery packs for grid storage. *Journal of Power Sources*, 195(8), 2377-2384.
- 466 [5] Kempton, W., & Letendre, S. E. (1997). Electric vehicles as a new power source for electric
467 utilities. *Transportation research. Part D, Transport and environment*, 2(3), 157-175.
- 468 [6] T. R. Hawkins et al., "Comparative Environmental Life Cycle Assessment of Conventional and
469 Electric Vehicles," *J. Ind. Ecol.* 17, 53 (2013).
- 470 [7] Woo, J., Choi, H., & Ahn, J. (2017). Well-to-wheel analysis of greenhouse gas emissions for
471 electric vehicles based on electricity generation mix: A global perspective. *Transportation
472 Research Part D: Transport and Environment*, 51, 340-350.
- 473 [8] Lowe, M., Tokuoka, S., Trigg, T., & Gereffi, G. (2010). Lithium-ion batteries for electric vehicles.
474 *The US Value Chain, Contributing CGGC researcher: Ansam Abayechi.*
- 475 [9] Du, J. and Ouyang, M., 2013, November. Review of electric vehicle technologies progress and
476 development prospect in China. In *Electric Vehicle Symposium and Exhibition (EVS27)*, 2013
477 World (pp. 1-8). IEEE.
- 478 [10] Wen X, Xiao C. Electric vehicle key technology research in China. In *Electrical Machines and
479 Power Electronics and 2011 Electromotion Joint Conference (ACEMP)*, 2011 International
480 Aegean Conference on 2011 Sep 8 (pp. 308-314). IEEE.
- 481 [11] Chen, X., Shen, W., Vo, T. T., Cao, Z., & Kapoor, A. (2012, December). An overview of lithium-
482 ion batteries for electric vehicles. In *IPEC, 2012 Conference on Power & Energy* (pp. 230-235).
483 IEEE.
- 484 [12] Iclodean, C., Varga, B., Burnete, N., Cimerdean, D., & Jurchiș, B. (2017, October). Comparison
485 of Different Battery Types for Electric Vehicles. In *IOP Conference Series: Materials Science and
486 Engineering* (Vol. 252, No. 1, p. 012058). IOP Publishing.
- 487 [13] Broussely, M., Planchat, J. P., Rigobert, G., Virey, D., & Sarre, G. (1997). Lithium-ion batteries
488 for electric vehicles: performances of 100 Ah cells. *Journal of power sources*, 68(1), 8-12.
- 489 [14] Lindgren, Juuso & Lund, P. (2016). Effect of extreme temperatures on battery charging and
490 performance of electric vehicles. *Journal of Power Sources*. 328. 37-45.
491 10.1016/j.jpowsour.2016.07.038.
- 492 [15] Leng, F., Tan, C. M., & Pecht, M. (2015). Effect of temperature on the aging rate of Li ion
493 battery operating above room temperature. *Scientific reports*, 5, 12967.
- 494 [16] Aris, A. M., & Shabani, B. (2017). An Experimental Study of a Lithium Ion Cell Operation at Low
495 Temperature Conditions. *Energy Procedia*, 110, 128-135.
- 496 [17] von Lüders, Christian, et al. "Lithium plating in lithium-ion batteries investigated by voltage
497 relaxation and in situ neutron diffraction." *Journal of Power Sources* 342 (2017): 17-23.
- 498 [18] Park, C., & Jaura, A. K. (2003). *Dynamic thermal model of li-ion battery for predictive behavior
499 in hybrid and fuel cell vehicles* (No. 2003-01-2286). SAE Technical Paper.
- 500 [19] Bhatia, P. C. (2013). Thermal analysis of lithium-ion battery packs and thermal management
501 solutions (Doctoral dissertation, The Ohio State University).
- 502 [20] Xia, G., Cao, L., & Bi, G. (2017). A review on battery thermal management in electric vehicle
503 application. *Journal of Power Sources*, 367, 90-105.
- 504 [21] De Vita, Armando, et al. "Transient thermal analysis of a lithium-ion battery pack comparing
505 different cooling solutions for automotive applications." *Applied Energy* 206 (2017): 101-112.

506 [22] Wang, Tao, et al. "Thermal investigation of lithium-ion battery module with different cell
507 arrangement structures and forced air-cooling strategies." *Applied energy* 134 (2014): 229-
508 238.

509 [23] Huber, C. (2017). *Phase Change Material in Battery Thermal Management Applications*
510 (Doctoral dissertation, Technische Universität München).

511 [24] Jaguemont, Joris, et al. "Phase-change materials (PCM) for automotive applications: a review."
512 *Applied Thermal Engineering* (2017).

513 [25] Liu, Huaqiang, et al. "Thermal issues about Li-ion batteries and recent progress in battery
514 thermal management systems: A review." *Energy Conversion and Management* 150 (2017):
515 304-330.

516 [26] Park H. A design of air flow configuration for cooling lithium ion battery in hybrid electric
517 vehicles[J]. *Journal of Power Sources*, 2013, 239:30-36.

518 [27] Xun J, Liu R, Jiao K. Numerical and analytical modeling of lithium ion battery thermal behaviors
519 with different cooling designs[J]. *Journal of Power Sources*, 2013, 233:47–61.

520 [28] Yang N, Zhang X, Li G, et al. Assessment of the forced air-cooling performance for cylindrical
521 lithium-ion battery packs: A comparative analysis between aligned and staggered cell
522 arrangements[J]. *Applied Thermal Engineering*, 2015, 80:55-65.

523 [29] Wang T, Tseng K J, Zhao J. Development of efficient air-cooling strategies for lithium-ion
524 battery module based on empirical heat source model[J]. *Applied Thermal Engineering*, 2015,
525 90:521-529.

526 [30] Li W, Xiao M, Peng X, Garg A, Gao L. A surrogate thermal modeling and parametric
527 optimization of battery pack with air cooling for EVs. *Applied Thermal Engineering*. 2019 Jan
528 25;147:90-100.

529 [31] Liao X, Ma C, Peng X, Garg A, Bao N. Temperature Distribution Optimization of an Air-Cooling
530 Lithium-Ion Battery Pack in Electric Vehicles Based on the Response Surface Method. *ASME.*
531 *J.Electrochem. En. Conv. Stor.*. 2019;16(4):041002-041002-8.

532 [32] Liu Yun, Sivasriprasanna Maddila, Liang Gao, Xiongbing Peng, Xiaodong Niu, Akhil Garg,
533 Christina May May Chin, "An integrated framework for minimization of inter lithium-ion cell
534 temperature differences and the total volume of the cell of battery pack for electric
535 vehicles", *Energy Storage*. 2019; 1:e41.

536 [33] Zhao J, Rao Z, Li Y. Thermal performance of mini-channel liquid cooled cylinder based battery
537 thermal management for cylindrical lithium-ion power battery[J]. *Energy Conversion &*
538 *Management*, 2015, 103:157-165.

539 [34] Huo Y, Rao Z, Liu X, et al. Investigation of power battery thermal management by using mini-
540 channel cold plate[J]. *Energy Conversion & Management*, 2015, 89:387-395.

541 [35] Hwang, H. Y., Chen, Y. S., & Chen, J. S. (2015). Optimizing the heat dissipation of an electric
542 vehicle battery pack. *Advances in Mechanical Engineering*, 7(1), 204131.

543 [36] Shui L, Chen F, Garg A, et al. Design optimization of battery pack enclosure for electric
544 vehicle[J]. *Structural & Multidisciplinary Optimization*, 2018(4):1-17.

545 [37] Fan L, Khodadadi J M, Pesaran A A. A parametric study on thermal management of an air-
546 cooled lithium-ion battery module for plug-in hybrid electric vehicles[J]. *Journal of Power*
547 *Sources*, 2013, 238: 301-312.

548 [38] Ling Z, Wang F, Fang X, et al. A hybrid thermal management system for lithium ion batteries
549 combining phase change materials with forced-air cooling[J]. *Applied energy*, 2015, 148: 403-
550 409.

551 [39] Chaturvedi, D. K. (2008). *Soft computing: techniques and its applications in electrical*
552 *engineering* (Vol. 103). Springer.

553
554
555
556
557